Open access • Journal Article • DOI:10.1021/ACS.CHEMMATER.8B03871

GeI2 Additive for High Optoelectronic Quality CsPbI3 Quantum Dots and Their Application in Photovoltaic Devices — Source link

Feng Liu, Chao Ding, Yaohong Zhang, Taichi Kamisaka ...+11 more authors

Institutions: University of Electro-Communications, National Renewable Energy Laboratory, University of Kitakyushu, Ritsumeikan University ...+2 more institutions

Published on: 12 Feb 2019 - Chemistry of Materials (American Chemical Society)

Topics: Quantum yield, Trioctylphosphine, Quantum dot, Yield (engineering) and Perovskite (structure)

GeI 2 additive for high optoelectronic quality CsPbI 3 quantum dots and their application in photovoltaic devices

CHEMISTRY OF MATERIALS

Article

GeI2 Additive for High Optoelectronic Quality CsPbI3 Quantum Dots and Their Application in Photovoltaic Devices

Feng Liu, Chao Ding, Yaohong Zhang, Taichi Kamisaka, Qian Zhao, Joseph M. Luther, Taro Toyoda, Shuzi Hayase, Takashi Minemoto, Kenji Yoshino, Bing Zhang, Songyuan Dai, Junke Jiang, Shuxia Tao, and Qing Shen

Chem. Mater., **Just Accepted Manuscript** • DOI: 10.1021/acs.chemmater.8b03871 • Publication Date (Web): 14 Jan 2019

GeI_2 Additive for High Optoelectronic Quality $CsPbI_3$ Quantum Dots and Their Application in Photovoltaic Devices

Feng Liu,[1] Chao Ding,[1] Yaohong Zhang,[1] Taichi Kamisaka,[1] Qian Zhao,[2,8] Joseph M. Luther,[2] Taro Toyoda,[1] Shuzi Hayase,[3] Takashi Minemoto,[4] Kenji Yoshino,[5] Bing Zhang,[6] Songyuan Dai,*[,6] Junke Jiang,[7] Shuxia Tao,[7] and Qing Shen*[,1]

[1]Faculty of Informatics and Engineering, The University of Electro-Communications, 1-5-1 Chofugaoka, Tokyo 182-8585, Japan

[2]National Renewable Energy Laboratory (NREL), Golden Colorado, 15013 Denver West Parkway, Golden 80401, USA

[3]Faculty of Life Science and Systems Engineering, Kyushu Institute of Technology, 2-4 Hibikino, Kitakyushu 808-0196, Japan

[4]Faculty of Science and Engineering, Ritsumeikan University, 1-1-1 Nojihigashi, Shiga 525-8577, Japan

[5]Department of Electrical and Electronic Engineering, Miyazaki University, 1-1 Gakuen, Miyazaki 889-2192, Japan

[6]Beijing Key Laboratory of Novel Thin Film Solar Cells, State Key Laboratory of Alternate Electrical Power System with Renewable Energy Sources, North China Electric Power University, Beijing 102206, P. R. China

[7]Center for Computational Energy Research, Department of Applied Physics, Eindhoven University of Technology, Eindhoven 5600 MB, The Netherlands

[8]College of Chemistry, Nankai University, Tianjin, P. R. China

Abstract

Trioctylphosphine (TOP)-based syntheses of $CsPbI_3$ perovskite quantum dots (QDs) yield unprecedented high photoluminescence quantum yield (PL QY), lower stokes shifts, and longer carrier lifetimes due to their enhanced crystallinity. This synthetic route relies on a heavily Pb-rich condition or a large Pb:Cs molar ratio in precursor solution to produce QDs with appropriate stoichiometry as well as to guarantee a good colloidal stability. The high Pb condition is achieved by a high concentration of PbI_2 prepared in TOP. Here we find such Pb-rich strategies can be avoided by

providing additional iodine ions using other metal halide salts. In particular GeI_2, which contrary to PbI_2, readily dissolves in TOP. $CsPbI_3$ QDs prepared using PbI_2/GeI_2 combination show near-unity PL QY and improved chemical stability compared to the previous synthetic route. Furthermore we find no sign of Ge incorporation in the QDs (compositionally or energetically). The ensuing QD solar cells deliver power conversion efficiency of 12.15% and retain 85% of its peak performance after storage over 90 days. The PbI_2/GeI_2 dual-source iodine synthetic approach presented here represents a more rational and robust route to high-quality $CsPbI_3$ QDs.

Introduction

Perovskites of the general formula ABX_3 (A = $CH_3NH_3^+$, $CH_3(NH_2)_2^+$, and Cs^+, B = Pb^{2+}, Sn^{2+}, Cu^{2+}, Bi^{3+}, and Sb^{3+}, X = Cl^-, Br^-, and I^-) are an important class of materials that have been extensively studied as promising candidates for light-harvesting as well as light-emitting applications.[1-6] These materials, and mainly the all-inorganic $CsPbI_3$ compound, have recently attracted intense research interest due to their suitable bandgap of 1.73 eV and improved phase/thermal stability in contrast to organic-inorganic hybrid counterparts.[7-11] However, the corner shared perovskite phase of $CsPbI_3$ is unstable in bulk as it prefers to change to the non-perovskite delta orthorhombic phase at room temperature.[12-17] To overcome this notable phase instability, $CsPbI_3$ perovskite has been processed into quantum dots (QDs). It was found that restricting the physical dimension of these semiconductor crystallites to a few nanometers greatly improves phase stability due to the large contribution of surface energy.[12, 15] Meanwhile, it also brings new attractive features, such as large spectral tunability and outstanding light emitting properties. Many groups across the world are now focused on synthesizing high-quality perovskite QDs and exploring their potential use in various applications.[13, 15, 18-30]

So far, there are several colloidal synthetic protocols established which lead to the formation of highly crystalline and size-tunable $CsPbI_3$ QDs.[14-15, 19, 28, 31-33] Among them, trioctylphosphine (TOP)-based synthetic methods recently proposed by our

group represent an efficient alternative to the traditional ways, whose QD product can approach near-unity photoluminescence quantum yield (PL QY) under optimized conditions due to their enhanced crystallinity.[28] However, our understanding of the parameters governing the successful synthesis of these nanocrystals is still very limited, a direct consequence of which is that, following those traditional synthetic approaches, an excessively high PbI_2 dissolved in TOP is often empirically determined. But on the other hand, lowering the use of PbI_2 to a certain degree will not lead to the successful synthesis of high-quality QDs with excellent colloidal stability and crystal quality. Such Pb-rich requirement brings daunting inconvenience and also causes a lot of toxic Pb waste.[28, 34] Unfortunately, the reason why excess PbI_2 is necessary and whether the use of PbI_2 can be reduced still remains unknown. The above questions drive us to gain more insight in the underlying precursors and reactions for the formation of $CsPbI_3$ QDs.

In this report, we elaborate on the synthesis of $CsPbI_3$ QDs, finding that Pb-rich conditions are actually not necessary for producing high-quality $CsPbI_3$ QDs and instead the excess iodide ions are what play a key role in stabilizing the final QDs. The reason why the traditional protocols as well as our TOP method need such a Pb-rich condition is because in these routes PbI_2 serves as the sole source of iodide ions, an excess PbI_2 is thus required to provide sufficient iodide ions to deactivate the reaction between Cs-oleate and $CsPbI_3$ QDs, the main detrimental process responsible for the failure of QD synthesis conducted under Cs-rich conditions. Based on the above guidelines, a new synthetic avenue was proposed which involves the use of other iodine salts, specifically here we use GeI_2, to serve as the robust source of iodide ions, thereby the demand for PbI_2 is greatly relieved. Other halide precursors such as ZnX_2, InX_3, NH_4X, and benzoyl halides have also been previously demonstrated for the synthesis of $CsPbX_3$, to improve PL QY and chemical stability of the $CsPbX_3$ QDs,[35-38] however, in these reports the Pb concentration (or Pb/Cs molar ratio) is still excessively high. We show here that use of metal halides which readily dissolve in TOP, removes the requirement that Pb must be in excess. This facilitates QD synthesis and reduces the amount of unreacted Pb-containing

precursors. Experimental results suggest that Ge is not incorporated into $CsPbI_3$ lattice, and hence does not affect the intrinsic properties of the resulting QDs. $CsPbI_3$ QDs prepared herein using PbI_2/GeI_2 precursor combination maintain a high crystalline quality with near-unity PL QY. Furthermore, they show better chemical stability than QD synthesized using only excessive PbI_2. We fabricate $CsPbI_3$ QD solar cells which exhibit power conversion efficiency (PCE) of 12.15% and retain 85% of its peak performance after storage in dry air over 90 days, showing great promise for practical use.

Results and Discussion

In TOP-based route to synthesizing $CsPbI_3$ QDs, PbI_2 dissolved in 2.5 mL TOP (0.6~1 mol/L, M) is rapidly injected into an octadecene solution containing Cs-oleate (0.75 mmol) at 120~180 °C.[28] $CsPbI_3$ QDs are generated presumably by the following reaction processes:

$$\text{TOP-PbI}_2 + 2\text{Cs-oleate} \rightarrow \text{Pb(oleate)}_2 + 2\text{CsI} + \text{TOP} \quad (1)$$

$$\text{CsI} + \text{TOP-PbI}_2 \rightarrow \text{CsPbI}_3\ (\text{QD}) + \text{TOP} \quad (2)$$

Reaction **1** produces the initial CsI crystals, which serve as the seed core for the formation of $CsPbI_3$ QDs by reacting with PbI_2 (*i.e.*, Reaction **2**). Overall, the formation of $CsPbI_3$ QDs can be described as follows:

$$2\text{Cs-oleate} + 3\text{PbI}_2 \rightarrow 2\text{CsPbI}_3\ (\text{QD}) + \text{Pb(oleate)}_2 \quad (3)$$

Accordingly, for complete reaction of both precursors, the Pb/Cs molar ratio must be ~1.5. However, empirically, for the sake of better colloidal stability and improved optoelectronic characteristics (such as unity PL QY), a Pb/Cs molar ratio of 2~2.6 in reaction mixture is typically used.[28] In fact, in previous traditional routes, this ratio is even higher (~4), which means that in both routes the PbI_2 is largely excessive, *i.e.*, the Pb-rich condition.[12, 15] In such conditions, unreacted PbI_2 and Pb-related byproducts remain.[34] For Pb/Cs molar ratio < 1.5, *i.e.*, the Cs-rich (or Cs-oleate-rich) condition, one may intuitively think the synthesis can also proceed with some Cs-related byproducts. However, unlike the Pb-rich conditions, reactions conducted at Pb/Cs molar ratio less than 1 do not lead to the formation of $CsPbI_3$ QDs and only a

white turbid suspension is obtained (see Figure S1a-b). Although Pb/Cs molar ratio at 1.1~1.5 can yield $CsPbI_3$ QDs, they decompose or transform quickly within a short period of time (5~10 min). The above facts point to a prerequisite in the synthesis that PbI_2 must be in excess.

In order to identify the mechanism behind the decomposition with lowered Pb/Cs molar ratios, we simulate a scenario using a neat $CsPbI_3$ QD solution which was prepared by a previous recipe.[28] As shown in Figure S1c-d, the neat $CsPbI_3$ QD solution gradually changes from red clear to white turbid with the addition of extra Cs-oleate, indicating the decomposition or transformation of the $CsPbI_3$ QDs. X-ray diffraction (XRD) technique was employed to monitor the substance produced at different stages. As shown in Figure S2, upon the addition of Cs-oleate, Cs_4PbI_6 crystal was first identified. A possible reaction for this can be written as follows:

$$CsPbI_3\ (QD) + \text{Cs-oleate} \rightarrow \frac{1}{2}Cs_4PbI_6 + \frac{1}{2}Pb(oleate)_2 \quad (4)$$

Further, with the increase in the addition of Cs-oleate, CsI precipitated out (Figure S3), which can be rationalized by the following reaction:

$$CsPbI_3\ (QD) + 2\text{Cs-oleate} \rightarrow 3CsI\ (\downarrow) + Pb(oleate)_2 \quad (5)$$

Bearing these in mind, we now turn to the formation process of $CsPbI_3$ QDs (Reaction **1-2**). If the above competitive reactions (Reaction **4**, **5)** take place in parallel to Reaction **1-2** and at a considerable rate, it would be indeed imperative to dissolve enough PbI_2, the sole source of iodine, to release sufficient iodide ions (I^-) to accelerate the reaction with Cs-oleate through: $I^- + Cs^+ = CsI$, *i.e.*, the essence of Reaction **1**, so as to alleviate the reaction between Cs-oleate and $CsPbI_3$ QDs.

One conclusion from the above deduction can be also drawn that the excess Pb^{2+} ions are in fact not essential for obtaining stable $CsPbI_3$ QDs as long as the iodide ions are sufficient to balance (or to consume) the excess Cs-oleate. In order to verify this notion, we design an I^--rich environment, where Pb^{2+} ions are set at a very low concentration. To do so, a mixture of GeI_2 and PbI_2 dissolved in TOP is prepared. The choice of GeI_2 to serve as the additional source of iodine is mainly because that superior to PbI_2, GeI_2 precursor solution with a high concentration can be readily

prepared in TOP. For example, dissolving 2 mmol of GeI_2 in 2.5 mL of TOP only takes 1~2 hours. The faster dissolution of GeI_2 in TOP may benefit from its stronger coordination ability with TOP due to acceptor and donor interaction.[39]

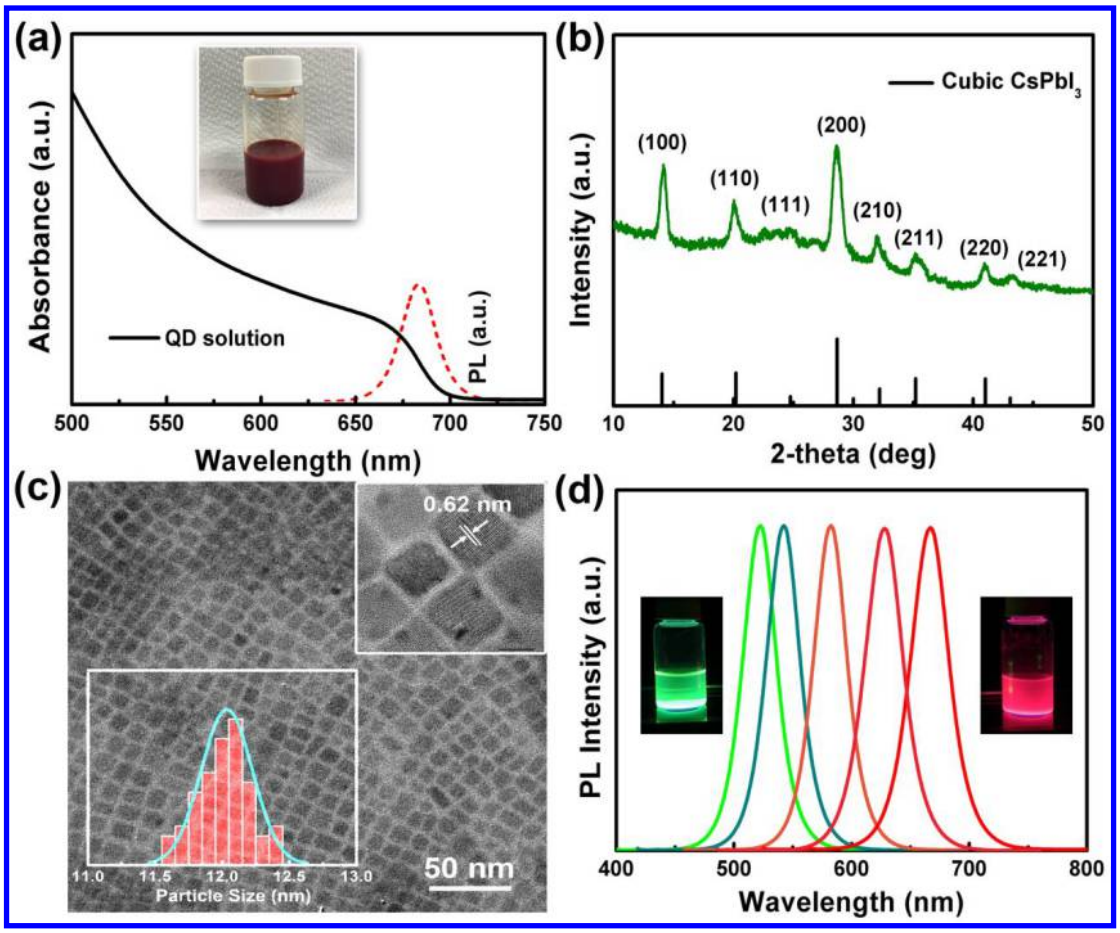

Figure 1. (a) Steady-state UV-vis absorption and PL emission spectra of the prepared QD solution. Full width at half maximum (FWHM) of the PL spectrum was about 33 nm. The inset shows a picture of a QD solution. (b) XRD patterns of the dried QD solution and a reference pure cubic-phase $CsPbI_3$ crystal. (c) HRTEM image of the QD sample. The inset graph shows statistical analysis of the size distribution while the inset image shows a zoomed-in image of the nanocrystals with well-resolved lattice fringes. (d) PL emission spectra of the QDs with different I/Br ratios synthesized at 180 °C (FWHM: 32~37 nm). The inset shows pictures of the two representative QD solutions taken under ultraviolet light.

Thus, a new synthetic approach using GeI_2/PbI_2 precursor mixture to high-quality $CsPbI_3$ QDs is described as follows: Briefly, 2.5 mL of TOP dissolved with 2 mmol

of GeI_2 and 0.5 mmol of PbI_2 is swiftly injected into an octadecene solution (12 mL) containing 0.75 mmol of Cs-oleate at 180 °C with vigorous stirring. Immediately upon injection, the solution changes from colorless to deep red, indicating nucleation and subsequent growth of the colloidal nanoparticles. The reaction was allowed to proceed for ~4 s after which the flask was rapidly cooled to room temperature. After synthesis, the QDs are washed with methyl acetate (MeOAc) to remove unreacted precursor and other synthesis products to yield a clean solution of $CsPbI_3$ QDs (more experimental details can be found in Supporting Information). We note the formation of Cs_4PbI_6 in the raw solution but these are mostly removed during this purification process (more details about the removal of Cs_4PbI_6 in the raw solution can be found in Figure S4, Supporting Information). It is important to mention that the added PbI_2 in TOP is now decreased to 0.2 M, which is significantly lower than that previously used (0.6~1 M), and the Pb/Cs molar ratio in reaction mixture is decreased to 0.66. We emphasize this is also the minimum value that $CsPbI_3$ QDs can be successfully produced, below which no $CsPbI_3$ QDs can be obtained (see Figure S5). Figure 1a shows UV-vis absorption and PL emission spectra of the resulting QDs. The sharp optical absorption edge (~670 nm) along with the narrow PL emission (~677 nm) suggest the successful synthesis of the $CsPbI_3$ QDs. XRD measurement was performed to examine crystal structure and phase purity of the resulting colloids. For XRD measurement, samples were prepared by dropping the purified solution on a glass substrate and dried by spin-casting. The main diffraction peaks at 14°, 20°, and 28.6° shown in Figure 1b confirm cubic-phase $CsPbI_3$ product. Figure 1c shows a representative high-resolution transmission electron microscopy (TEM) image of the purified sample, where uniform cubic-shaped dots (average size of ~12 nm) with well-resolved lattice fringes (interplanar spacing of 0.62 nm) can be clearly identified, indicating highly crystalline structure of the resulting $CsPbI_3$ QDs.

The above experimental results unambiguously show that $CsPbI_3$ QDs can be successfully synthesized even under a low concentration of PbI_2 (3 to 4-fold decrease as compared with before) by using a combined Ge/Pb precursor. One additional merit using the Ge salt additives is that it now enables preparation of $CsPbX_3$ QDs with

various halide compositions, and because of which a wider range of luminescence emission can be obtained (see Supporting Information for more synthetic details). Indeed, the efficacy of the previous strategy employing PbX_2 alone for the synthesis of different halide compositions is largely limited because of the extremely low solubility of $PbBr_2$ in TOP (<< 0.1 mol/L). In contrast, Ge halide compounds can provide sufficient bromide ions to the reaction due to their higher solubility in TOP. Figure 1d displays that $CsPbX_3$ QDs prepared using different $PbI_2/GeI_2/GeBr_2$ combinations exhibit photoluminescence from 520 to 677 nm and show bright fluorescence under ultraviolet light (the detailed synthesis conditions for each PL spectrum were given in Table S1).

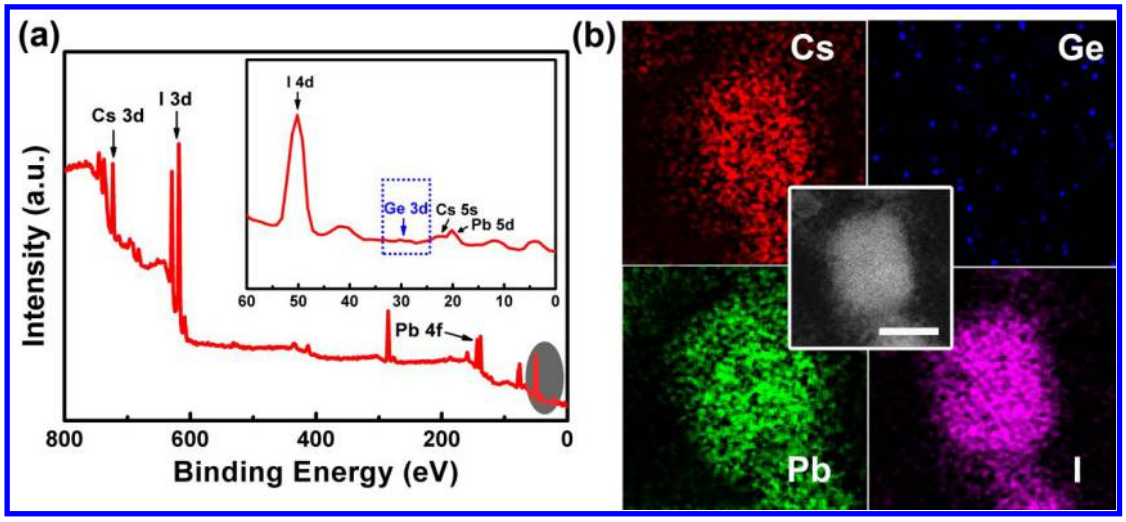

Figure 2. (a) Wide-scan XPS spectra of the resulting QDs. Inset displays an enlarged view from 0~60 eV. (b) TEM image and EDX microanalysis mapping of a single QD. The scale bar represents 10 nm.

Using the dual halide source precursor (GeI_2/PbI_2), we question whether the Ge element is present in the final QDs. Previous studies using Zn salts in hot-injection synthesis reported no incorporation of Zn^{2+} in their samples.[37-38] We therefore suspect Ge to behave similarly, but nonetheless probe to see if we can find evidence of it. To examine the composition and valence state of the constituent elements, X-ray photoelectron spectroscopy (XPS) measurement was carried out. As shown in Figure 2a, XPS peaks assignable to Cs(I) 3d, Pb(II) 4f, and I(I) 3d can be clearly identified. However, Ge signals typically appear in the range of 25~35 eV,[40] and no clear XPS

peaks can be resolved in that range. This indicates that the washed QD product contains negligible amount of the Ge element. TEM-energy dispersive X-ray microanalysis (TEM-EDX) was further conducted to confirm this result. As can be seen from Figure 2b, Cs, Pb, and I elements are homogeneously distributed throughout the QD while for the Ge element, EDX does not have the necessary signal to noise ratio to be considered processible, confirming that Ge element is indeed not present in the final QDs and the resulting colloids are basically $CsPbI_3$ QDs. In order to investigate the potential role of GeI_2 in the synthesis besides the identified role of I^- source, we then carried out XPS measurement to study the chemical state of Ge in the solution after reaction. Details about sample preparation can be found in caption of Figure S6. Figure S6 shows that binding energy of Ge 3d after synthesis is not significantly changed as compared to that of the as-bought GeI_2 powder, indicating that the chemical state of Ge is not affected during reaction. Therefore, from the above results, we can safely conclude that GeI_2 serves only as a source of I^- during formation of $CsPbI_3$ QDs.

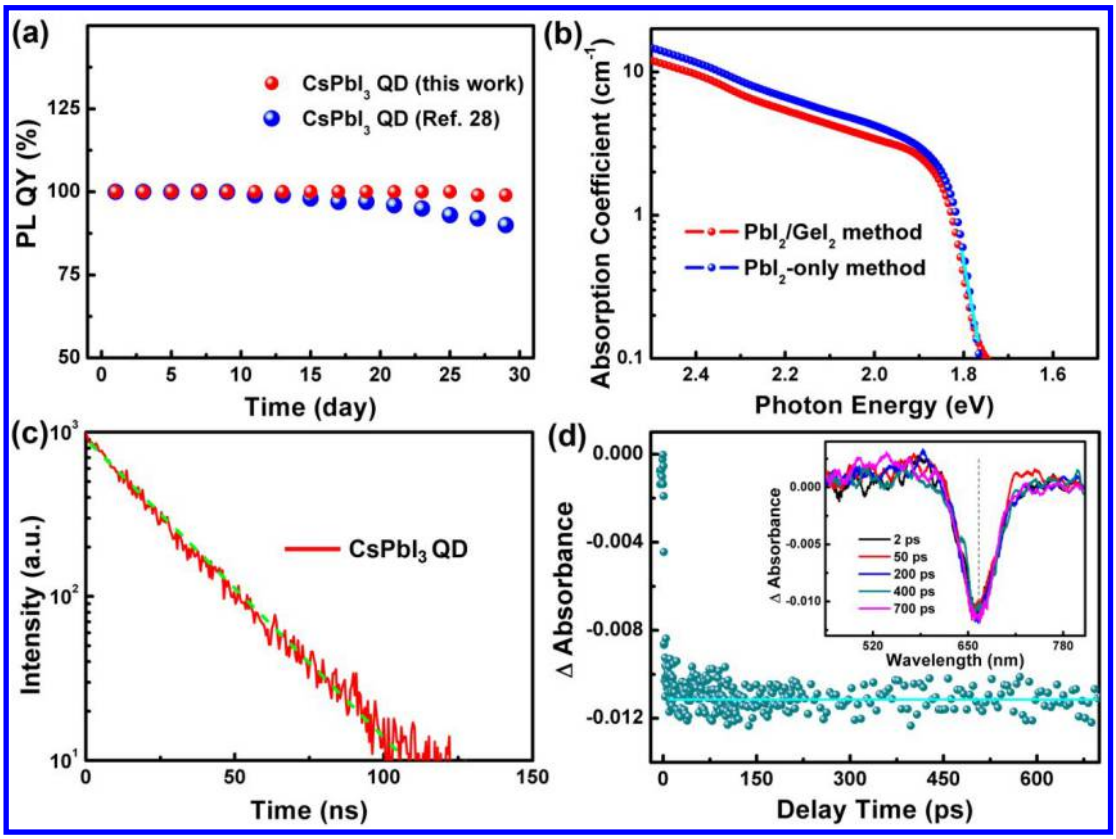

Figure 3. (a) Evolution of the PL QY of the prepared QD solutions over storage time.

Dotted red: PbI_2/GeI_2-produced $CsPbI_3$ QDs. Dotted blue: excessive PbI_2-produced QDs (Ref. 28). Both QDs were synthesized at 180 °C, washed once with 122 mL of MeOAc and stored in a sealed bottle with air at room temperature. (b) Absorption coefficient of the $CsPbI_3$ QDs prepared using PbI_2/GeI_2 combination method versus only PbI_2 (Ref. 28) (particle size ~12 nm). (c) Time-resolved PL decay curves of the $CsPbI_3$ QDs. Pump intensity and wavelength are 0.29 mW and 532 nm, respectively. (d) TA kinetic traces of the $CsPbI_3$ QDs. TA spectra were recorded with excitation wavelength of 470 nm, excitation intensity of 1 $\mu J/cm^2$, and probe wavelength of ~670 nm. The inset shows TA spectra recorded at different delay times.

Photophysical properties of the resulting $CsPbI_3$ QDs were first evaluated by measuring their PL QYs using a commercial Hamamatsu setup (details about the measurement principle can be found in Figure S7). Amazingly, high PL QY of nearly 100% is achieved for these $CsPbI_3$ QDs prepared under such a low PbI_2 concentration (A histogram of the PL QY values for 14 batches of syntheses is presented in Figure S8). This means that the intrinsic decay channel of the excited states in these QDs is also nearly completely radiative. More importantly, QDs show PL QY of 99±2% even after 1 month storage (Figure 3a). In contrast, those $CsPbI_3$ QDs prepared using only excessive PbI_2 as described in our previous method (Ref. 28) can only maintain PL QY of 100±2% for the first 9 days and dropped to ~85±2% after storage for 1 month. In order to gain more insight about the superior photophysical properties of the QDs produced by PbI_2/GeI_2 method, XPS measurement was carried out. XPS measurements have been widely used to assess the surface modification of the QDs[41] and to understand the mechanism of PL enhancement. Quantitative XPS analysis for QDs produced by PbI_2/GeI_2 method indicates a I/Pb ratio of 4.0±0.2, which is higher than that of the stoichiometry in the bulk (I/Pb ratio = 3) (note that the measured QD samples have been sufficiently purified with MeOAc after synthesis). The excess iodine may come from the capping ligands on QD surface, oleylammonium iodide, which helps to passivate the surface defects.[11, 27, 42] Further, as a comparison, we carried out quantitative XPS analysis on QDs prepared by PbI_2-only method, I/Pb

ratio turns out to be 3.3±0.2, which is lower than that prepared by PbI_2/GeI_2 method. The stable high PL QY makes the synthesized QDs highly suitable for many applications, including biological labeling, LEDs, photovoltaics, and lasers. Further, small Urbach energy (E_U) ~19 meV calculated by a reference method is also obtained from Figure 3b, which is close to that of the QDs prepared by PbI_2-based method of similar particle size. The measured low E_U value is a strong sign that the QDs suffer less from impurities, inherent structural disorders, and electron-phonon interaction in their light-absorption process.[43-45] PL decay measurement probing the PL maximum (~677 nm) shows these 12 nm-$CsPbI_3$ QDs exhibit spectrally uniform single-exponential decay with a 22 ns time constant (Figure 3c), which implies a single recombination channel across the entire QD ensemble. The above results thus confirm that lowering the use of PbI_2 does not necessarily impair the intrinsic properties of $CsPbI_3$ QDs, instead, the resulting QDs can still maintain a low level of electronic disorder and/or defect density, and therefore an excellent crystalline nature. However, unlike the $CsPbI_3$ QDs, it should be mentioned that the prepared $CsPb(I/Br)_3$ QDs using PbI_2/$GeBr_2$ combination do not show PL QY as high as 100±2%. In fact, PL QY of the $CsPb(I/Br)_3$ QDs significantly decreased from 100±2% to 40±2% with the increase in Br content. It should be mentioned that the decrease of PL QY of the perovskite QDs when using mixed halides is not exclusive to this work. For example, in Ahmed *et al.*'s report, the directly synthesized $CsPbBr_3$ and $CsPbI_3$ QDs exhibit PL QY of ~30% and ~40%, respectively, while that of $CsPbI_{3-x}Br_x$ is 10~13%.[11] In our own experience following a universal synthetic method,[15] under optimal conditions, we can achieve PL QY of ~90% for $CsPbI_3$ QDs and ~80% for $CsPbBr_3$ QDs, however, PL QY of $CsPbI_{3-x}Br_x$ is typically lower, being 50~70%. Similar observation is also reported by Liu *et al.*.[46] These experimental results indicate that the mixed halide source synthesis could induce remarkable formation of lattice/surface defects that would lead to deterioration of the optical properties of the QDs.

The successful application of GeI_2 in the synthesis of high-quality $CsPbI_3$ QDs drives us to explore the efficacy of the other metal halides, such as CuI, HgI_2, ZnI_2,

AgI, NH_4I, and SrI_2. We found that all these studied metal halides can be readily dissolved in TOP with a high concentration (~0.8 M) except for SrI_2 (< 0.1 M) and NH_4I (< 0.2 M). However, among these dissoluble metal halides, only ZnI_2 can lead to the successful synthesis of $CsPbI_3$ QDs (Figure S9). Yet compared to QD prepared with GeI_2, the ZnI_2-based $CsPbI_3$ QDs show lower PL QY (~50±2%) and less colloidal stability. The reason behind this observation is still under investigation; however, we consider the difference in the ability of these metal salts to release reactive iodide ions could probably account for these. The above fact also indicates that the compensatory halide precursor used in TOP route is highly selective.

Femtosecond transient absorption (TA) measurement was performed to elucidate the mechanism underlying the superb photophysical properties of the resulting $CsPbI_3$ QDs prepared using PbI_2/GeI_2 combination. Upon band gap excitation of the QDs with light pulse, one can see bleaching signal (absorption changes $\Delta A < 0$) in its TA spectrum, which corresponds to state filling by electrons and/or holes in the QDs.[47] In the absence of charge transfer between QDs or a charge acceptor, the recovery of the transient bleach or depletion of the absorption signal near band gap of the QDs represents the disappearance of the photogenerated electrons and/or holes *via* charge recombination and trapping processes within a single QD.[48-49] Therefore, TA measurement can serve as a measure of the trap states in the QDs. But before carrying out analysis of trap states using TA measurement, Auger recombination in $CsPbI_3$ QDs is first studied and eliminated because the Auger recombination time scale could potentially overlap with that of the charge trapping process and tend to complicate the discussion.[50-53] Figure S10 shows the dependence of the normalized TA decays on pump excitation intensities for the measured QDs. It is clearly seen that the decay process becomes fast when the pump intensity is larger than 2 $\mu J/cm^2$. This observation indicates the presence of Auger recombination process in QDs under the high pump intensity excitation.[53] When the pump intensity is smaller than 2 $\mu J/cm^2$, we found the fast decay process disappeared and the waveforms of the TA responses overlapped with each other very well within 1 ns when they were normalized at the peak intensity. This means the Auger recombination process is negligible under such

low pump intensity excitation. Therefore, in the following, for the TA measurements, QD samples will be excited with a safe pump intensity of 1 μJ/cm^2 to eliminate the potential interference of Auger process. Figure 3d shows TA response of the $CsPbI_3$ QDs measured with pump intensity of 1 μJ/cm^2, where no significant decay can be resolved in the initial 1 ns time scale, suggesting the negligible electron or hole trapping pathways in the QDs.

In order to apply these high-quality colloidal QDs into high-performance photovoltaics or light emitting diodes, it is typically required to process them into compact thin films so as to enable an efficient charge transfer between nanoparticles. Here, QD compact thin films with a controllable thickness were prepared by a modified deposition process, which was initially developed for making high-efficiency $CsPbI_3$ QD solar cells.[12, 54] Specifically, in a N_2-filled glovebox, 100 μL of QD solution (~60 mg/mL) was first deposited on a fluorine-doped tin oxide (FTO) glass by spin casting at 3600 rpm for 20 s. Then the as-cast QDs were treated 5~6 times with MeOAc, in each treatment, QD surface was flooded with MeOAc, left for ~1 s and dried at 3600 rpm for 20 s. The above QD deposition-MeOAc washing process is defined as one cycle of QD deposition and it can be repeated several cycles to produce dense films with a desired thickness. Figure S11a shows a typical cross-section scanning electron microscope (SEM) image of a prepared QD thin film, where a 200-nm-thick compact QD layer can be clearly identified on the FTO substrate. Comparison of the Fourier-transform infrared (FT-IR) spectra of the QD films as cast and after treatment with MeOAc suggests the further removal of the organic species from the QDs, given that those C-H bending vibration peaks at 2853 and 2923 cm^{-1} assignable to the hydrocarbon chains from organics are significantly reduced (Figure S11b).[41]

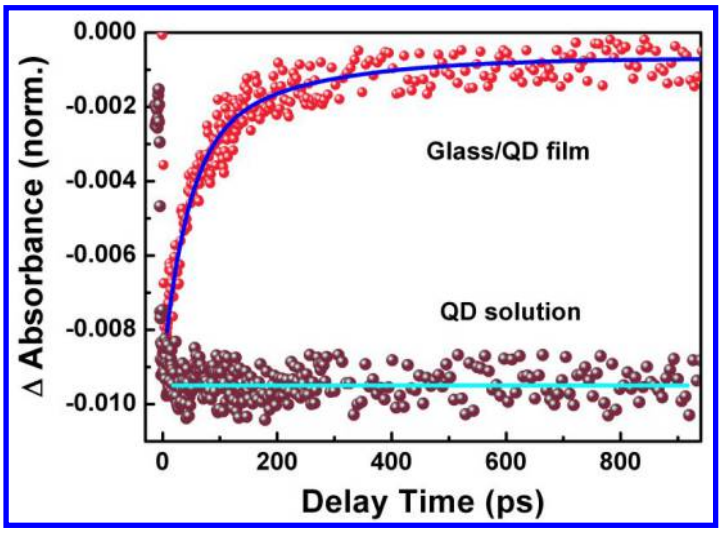

Figure 4. TA kinetic traces of the QD dense films and those dispersed in solution. Excitation wavelength is 470 nm and power intensity is 1 μJ/cm^2. Solid line shows fit to the TA dynamics.

As mentioned above, free-standing QDs are processed into dense thin films to enable their electrical contact and thus allow an efficient charge transfer between nanoparticles. First evidence of the efficient charge transfer between QDs comes from steady-state PL spectra, from which we can see the intrinsic fluorescence of the QDs was significantly quenched in the films (Figure S12). To obtain direct evidence of the charge transfer and, furthermore, to evaluate the rate of this process, next, again, TA spectroscopy was employed. For TA measurement, QD dense films were prepared on a quartz glass and QDs dispersed in solution were used as reference. Both were excited with wavelength of 470 nm and power intensity of 1 μJ/cm^2 (Figure S13a shows that under this low power intensity the Auger recombination in QD thin film is negligible). Normalized TA kinetics at the bleach maximum were recorded for each sample as shown in Figure 4. It should be mentioned that the TA bleach maximum of the free QD solution is located at ~670 nm, while that of QD thin film sample is located at ~685 nm. This red shift may result from some degree of attachment after MeOAc treatment, which results in a decrease in the averaged QD-QD distance and causes a change in the dielectric environment of the surface bound QDs when compared to the solution, and eventually affects the total energy of an exciton confined to the QDs.[55-57] It is seen that compared to the non-decay TA kinetic features

observed for those QDs dispersed in solution, TA response of the thin films shows fast decay within 1 ns. This is indicative of charge transfer between QDs. Fitting of the TA response of the QD thin films gives single-exponential decay kinetics (*i.e.*, $A_0\exp(-t/\tau) + y_0$) with time constant of ~50 ps ($A_0 \approx 90\%$) and $y_0 \approx 10\%$. The derived fast decay component thus reveals that the photoexcited charge carriers in QDs can transport between each other with a fast transfer rate (k_{et}) of 0.2×10^{11} s^{-1} ($k_{et} = 1/\tau$). It is important to bear in mind, however, that the decay of TA signal can be also related to surface trapping defects with a close lifetime to that of charge transfer since $CsPbI_3$ QDs have underwent a severe surface treatment with MeOAc during thin film deposition, surface trapping defects can be formed and contribute to decay of TA signal. However, due to their close lifetime constant, it is difficult to quantitatively estimate the contribution of these two different processes to the TA decay. In order to gain more insight into the presence of trap states in QD thin films, we obtained spectro-temporal TA map for $CsPbI_3$ QD thin films, as shown in Figure S13b. The red shift of the bandedge bleach maximum with time in a spectro-temporal TA map correlates to a certain degree of disorder with energy funnelling towards undesired bandtail states, it can be thus tracked as a sign of trap states below the bandgap.[58] A very small redshift ~3 meV of the transient bleach peak is observed for the investigated $CsPbI_3$ QD thin film, suggesting a flat energy landscape and a very shallow trap below the bandgap. Given such a shallow trap state reflected here, we consider TA decay near band gap of the QDs is dominated by charge transfer process between QDs.

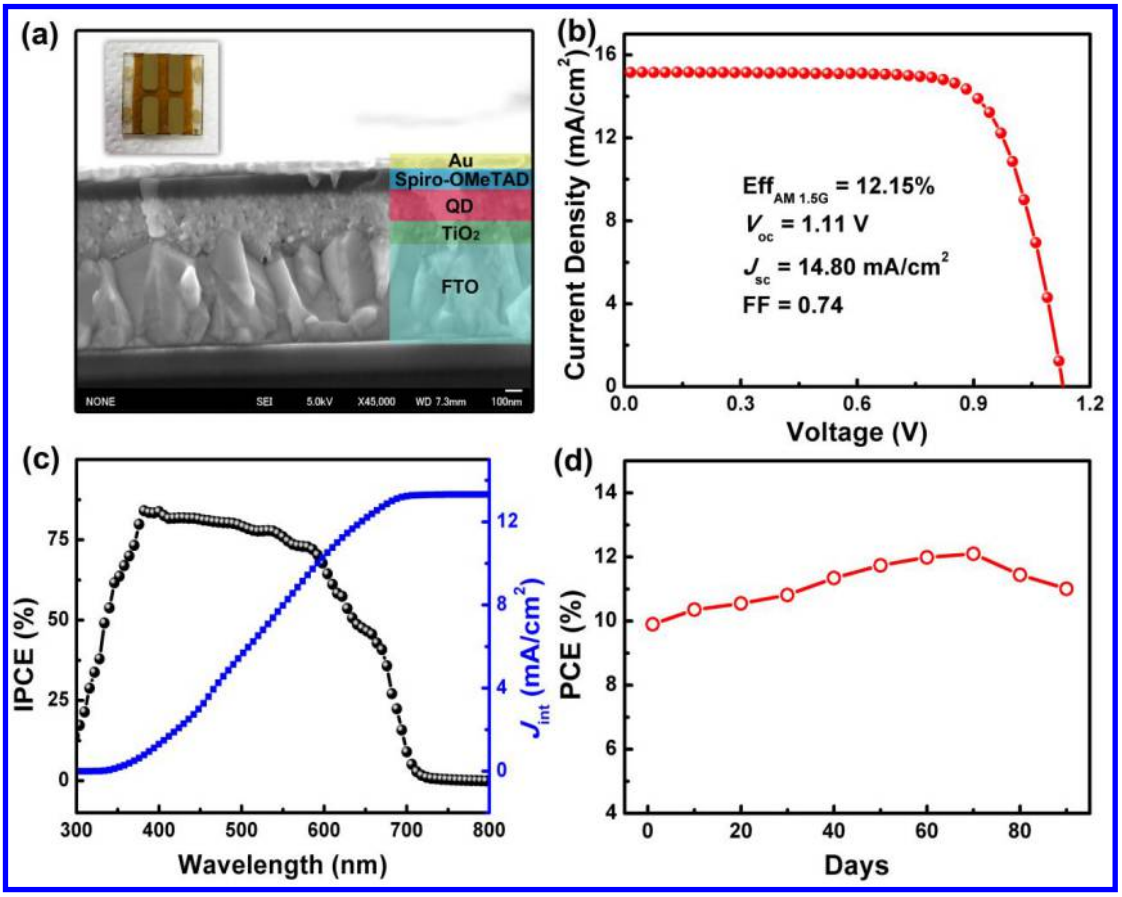

Figure 5. (a) Cross-sectional SEM image of the fabricated solar cells. (b) Current density-voltage (*J-V*) curves of the champion QD perovskite solar cells measured under simulated solar illumination of 100 mW/cm^2. (c) IPCE spectrum and integrated photocurrent density for the best-performing solar cell. (d) Long-term device stability measurement of the solar cells. The unsealed solar cells were kept in a dry cabinet (< 20% relative humidity) in the dark under room temperature and tested regularly in open air with the relative humidity of 30~40%. PCE values were obtained from the reverse scans.

The efficient charge transfer between QDs enabled by the thin films renders these materials extremely suitable for use in thin film solar cells. Hall measurements reveal that the prepared QD thin films exhibit p-type conducting behavior with a carrier concentration of 1.28 × 10^{13} cm^{-3} and mobility of 22.95 cm^2/Vs. The valence band maximum of the $CsPbI_3$ QDs about -5.25 eV was revealed by photoelectron yield spectroscopy (PYS) measurement, as shown in Figure S14. Band alignment between the QDs and the other layers is shown in the inset of Figure S14, which demonstrates

an energetically favorable band position for the transfer of the photoexcited electrons and holes from QDs to TiO_2 and Spiro-OMeTAD, respectively. We therefore fabricated $CsPbI_3$ QD planar solar cells using a thin layer of TiO_2 as the electron-acceptor and Spiro-OMeTAD as the hole-transporting layer (detailed fabrication process can be found in Supporting Information). Figure 5a shows a typical SEM image of the cross section of the fabricated solar cells. The best-performing QD solar cell with an optimal QD layer thickness of ~220 nm tested under ambient conditions delivers a PCE of 12.15% (Figure 5b) with hysteresis behavior shown in Figure S15. This is one of the highest efficiency among all-inorganic perovskite solar cells reported so far. A histogram of the PCE values for 28 samples is presented in Figure S16. Integrating the incident photon conversion efficiency (IPCE) data with the AM 1.5G solar spectrum gives calculated short-circuit current density (J_{sc}) value of approximately 13.5 mA/cm^2 (Figure 5c), which is in good agreement with the experimental value obtained from *J-V* measurement. We also examined the long-term stability of the solar cells under dark storage in dry air (room temperature, < 20% relative humidity). As shown in Figure 5d, the PCE of the solar cells as determined from reverse *J-V* scans increased from its initial value over the course of 60 days and retained 85% of its peak performance after 90 days, showing superior stability in dry air. However, when these QD devices are taken out and exposed to ambient conditions of a typical day-night cycle (~25 °C, relative humidity of 30~40%), the efficiency decreases to ~2.5% (Figure S17a), similar to that reported previously.[12] The main cause of this dramatic drop in efficiency is attributed to the known phase transformation of cubic $CsPbI_3$ to 2D orthorhombic $CsPbI_3$. Figure S17b shows that light absorption of the QD film has significantly changed after storage in air for one day, in line with transformation of the phase. We have also fabricated solar cells using $CsPbI_3$ QDs that were prepared with no GeI_2. PCE and stability of the solar cells are summarized in Figure S18. It is observed that efficiency of the solar cells increased in the first three weeks from ~9.0% to ~9.9%, and decreased to ~9.2% after ~30 days storage in dark dry box. Compared to QD devices prepared with GeI_2, the photovoltaic performance and stability of the solar cells with

no GeI_2 is slightly lower. The reason behind this can be due to a better surface passivation of the QDs produced in PbI_2/GeI_2 route, as revealed by quantitative XPS measurement for PL QY comparison.

Conclusions

In conclusion, we have presented a new synthetic strategy by introducing GeI_2 as an additional robust source of iodide ions, the use of PbI_2 can be thus greatly reduced, which brings significant advantages, such as less toxic Pb waste, better surface passivation of the QDs, and better reproducibility of the products. The resulting $CsPbI_3$ QDs synthesized with PbI_2/GeI_2 precursor combination show near-unity PL QY as well as improved chemical stability, and the ensuing QD solar cells exhibit high PCE over 12%. Therefore, the PbI_2/GeI_2 dual-source iodine synthesis approach introduced here shall represent a more rational and efficient route to high-quality $CsPbI_3$ QDs.

Associated Content

Supporting Information

Experimental details, solution picture, XRD, SEM images, PL QY measurement, TA spectra, PL spectra, PYS, *J-V* curves.

Author Information

Corresponding Authors

shen@pc.uec.ac.jp

sydai@ncepu.edu.cn

Author Contributions

F.L. synthesized the QDs, C.D., Y.Z., and Q.Z. fabricated devices. All authors contributed to QD or device characterization, analysis, figures, and edits to the manuscript.

Notes

The authors declare no competing financial interest.

Acknowledgements

This research was supported by the Japan Science and Technology Agency (JST) CREST program, JST PRESTO program, the MEXT KAKENHI Grant (Grant Number 26286013, 17H02736), JSPS International Research Fellow (Faculty of Informatics and Engineering, UEC). This work was authored in part by Alliance for Sustainable Energy, LLC, the manager and operator of the National Renewable Energy Laboratory for the U.S. Department of Energy (DOE) under Contract No. DE-AC36-08GO28308. Funding for J.M.L. provided by the Laboratory Directed Research and Development (LDRD) program at NREL. Q.Z. acknowledges fellowship support from the China Scholarship Council.

References

1. Lu, J.; Lin, X.; Jiao, X.; Gengenbach, T.; Scully, A. D.; Jiang, L.; Tan, B.; Sun, J.; Li, B.; Pai, N.; Bach, U.; Simonov, A. N.; Cheng, Y.-B., Interfacial Benzenethiol Modification Facilitates Charge Transfer and Improves Stability of cm-Sized Metal Halide Perovskite Solar Cells with Up to 20% Efficiency. *Energy Environ. Sci.* **2018,** *11*, 1880-1889.

2. McMeekin, D. P.; Sadoughi, G.; Rehman, W.; Eperon, G. E.; Saliba, M.; Horantner, M. T.; Haghighirad, A.; Sakai, N.; Korte, L.; Rech, B.; Johnston, M. B.; Herz, L. M.; Snaith, H. J., A Mixed-Cation Lead Mixed-Halide Perovskite Absorber for Tandem Solar Cells. *Science* **2016,** *351*, 151-155.

3. Bi, D. Q.; Tress, W.; Dar, M. I.; Gao, P.; Luo, J. S.; Renevier, C.; Schenk, K.; Abate, A.; Giordano, F.; Baena, J. P. C.; Decoppet, J. D.; Zakeeruddin, S. M.; Nazeeruddin, M. K.; Gratzel, M.; Hagfeldt, A., Efficient Luminescent Solar Cells Based on Tailored Mixed-Cation Perovskites. *Sci. Adv.* **2016,** *2*, e1501170.

4. Ravi, V. K.; Scheidt, R. A.; DuBose, J.; Kamat, P. V., Hierarchical Arrays of Cesium Lead Halide Perovskite Nanocrystals through Electrophoretic Deposition. *J. Am. Chem. Soc.* **2018,** *140*, 8887-8894.

5. Palazon, F.; Di Stasio, F.; Akkerman, Q. A.; Krahne, R.; Prato, M.; Manna, L., Polymer-Free Films of Inorganic Halide Perovskite Nanocrystals as UV-to-White Color-Conversion Layers in LEDs. *Chem. Mater.* **2016,** *28*, 2902-2906.

6. Yakunin, S.; Protesescu, L.; Krieg, F.; Bodnarchuk, M. I.; Nedelcu, G.; Humer, M.; De Luca, G.; Fiebig, M.; Heiss, W.; Kovalenko, M. V., Low-Threshold Amplified Spontaneous Emission and Lasing from Colloidal Nanocrystals of Caesium Lead Halide Perovskites. *Nat. Commun.* **2015,** *6*, 8056.

7. Ma, Q. S.; Huang, S. J.; Wen, X. M.; Green, M. A.; Ho-Baillie, A. W. Y., Hole Transport Layer Free Inorganic CsPbIBr2 Perovskite Solar Cell by Dual Source Thermal Evaporation. *Adv. Energy Mater.* **2016,** *6*, 1502202.

8. Wang, Q.; Jin, Z.; Chen, D.; Bai, D.; Bian, H.; Sun, J.; Zhu, G.; Wang, G.; Liu, S., μ-Graphene Crosslinked CsPbI3 Quantum Dots for High Efficiency Solar Cells with Much Improved Stability. *Adv. Energy Mater.* **2018**, 1800007.

9. Zhang, J.; Bai, D.; Jin, Z.; Bian, H.; Wang, K.; Sun, J.; Wang, Q.; Liu, S., 3D–2D–0D Interface Profiling for Record Efficiency All-Inorganic CsPbBrI2 Perovskite Solar Cells with Superior Stability. *Adv. Energy Mater.* **2018,** *8*, 1703246.

10. Sutton, R. J.; Eperon, G. E.; Miranda, L.; Parrott, E. S.; Kamino, B. A.; Patel, J. B.; Hörantner, M. T.; Johnston, M. B.; Haghighirad, A. A.; Moore, D. T., Bandgap-Tunable Cesium Lead Halide Perovskites with High Thermal Stability for Efficient Solar Cells. *Adv. Energy Mater.* **2016,** *6*, 1502458.

11. Ahmed, T.; Seth, S.; Samanta, A., Boosting the Photoluminescence of CsPbX3 (X = Cl, Br, I) Perovskite Nanocrystals Covering a Wide Wavelength Range by Postsynthetic Treatment with Tetrafluoroborate Salts. *Chem. Mater.* **2018,** *30*, 3633-3637.

12. Swarnkar, A.; Marshall, A. R.; Sanehira, E. M.; Chernomordik, B. D.; Moore, D. T.; Christians, J. A.; Chakrabarti, T.; Luther, J. M., Quantum Dot-Induced Phase Stabilization of Alpha-CsPbI3 Perovskite for High-Efficiency Photovoltaics. *Science* **2016,** *354*, 92-95.

13. Akkerman, Q. A.; Rainò, G.; Kovalenko, M. V.; Manna, L., Genesis, Challenges and Opportunities for Colloidal Lead Halide Perovskite Nanocrystals. *Nat. Mater.* **2018,** *17*, 394-405.

14. Lu, C.; Li, H.; Kolodziejski, K.; Dun, C.; Huang, W.; Carroll, D.; Geyer, S. M., Enhanced Stabilization of Inorganic Cesium Lead Triiodide (CsPbI3) Perovskite

Quantum Dots with Tri-octylphosphine. *Nano Res.* **2018,** *11*, 762-768.

15. Protesescu, L.; Yakunin, S.; Bodnarchuk, M. I.; Krieg, F.; Caputo, R.; Hendon, C. H.; Yang, R. X.; Walsh, A.; Kovalenko, M. V., Nanocrystals of Cesium Lead Halide Perovskites (CsPbX3, X = Cl, Br, and I): Novel Optoelectronic Materials Showing Bright Emission with Wide Color Gamut. *Nano Lett.* **2015,** *15*, 3692-3696.

16. Zhao, B.; Jin, S.; Huang, S.; Liu, N.; Ma, J.-Y.; Xue, D.-J.; Han, Q.; Ding, J.; Ge, Q.-Q.; Feng, Y.; Hu, J.-S., Thermodynamically Stable Orthorhombic γ-CsPbI3 Thin Films for High-Performance Photovoltaics. *J. Am. Chem. Soc.* **2018**, 11716-11725.

17. Sun, J.-K.; Huang, S.; Liu, X.-Z.; Xu, Q.; Zhang, Q.-H.; Jiang, W.-J.; Xue, D.-J.; Xu, J.-C.; Ma, J.-Y.; Ding, J.; Ge, Q.-Q.; Gu, L.; Fang, X.-H.; Zhong, H.-Z.; Hu, J.-S.; Wan, L.-J., Polar Solvent Induced Lattice Distortion of Cubic CsPbI3 Nanocubes and Hierarchical Self-Assembly into Orthorhombic Single-Crystalline Nanowires. *J. Am. Chem. Soc.* **2018**, 11705-11715.

18. Song, J.; Li, J.; Li, X.; Xu, L.; Dong, Y.; Zeng, H., Quantum Dot Light-Emitting Diodes Based on Inorganic Perovskite Cesium Lead Halides (CsPbX3). *Adv. Mater.* **2015,** *27*, 7162-7167.

19. Sun, S. B.; Yuan, D.; Xu, Y.; Wang, A. F.; Deng, Z. T., Ligand-Mediated Synthesis of Shape-Controlled Cesium Lead Halide Perovskite Nanocrystals via Reprecipitation Process at Room Temperature. *ACS Nano* **2016,** *10*, 3648-3657.

20. Pan, A. Z.; He, B.; Fan, X. Y.; Liu, Z. K.; Urban, J. J.; Alivisatos, A. P.; He, L.; Liu, Y., Insight into the Ligand-Mediated Synthesis of Colloidal CsPbBr3 Perovskite Nanocrystals: The Role of Organic Acid, Base, and Cesium Precursors. *ACS Nano* **2016,** *10*, 7943-7954.

21. Protesescu, L.; Yakunin, S.; Bodnarchuk, M. I.; Bertolotti, F.; Masciocchi, N.; Guagliardi, A.; Kovalenko, M. V., Monodisperse Formamidinium Lead Bromide Nanocrystals with Bright and Stable Green Photoluminescence. *J. Am. Chem. Soc.* **2016,** *138*, 14202-14205.

22. Liu, Z.; Bekenstein, Y.; Ye, X.; Nguyen, S. C.; Swabeck, J.; Zhang, D.; Lee, S.-T.; Yang, P.; Ma, W.; Alivisatos, A. P., Ligand Mediated Transformation of Cesium Lead Bromide Perovskite Nanocrystals to Lead Depleted Cs4PbBr6

Nanocrystals. *J. Am. Chem. Soc* **2017,** *139*, 5309-5312.

23. Liu, W.; Lin, Q.; Li, H.; Wu, K.; Robel, I.; Pietryga, J. M.; Klimov, V. I., Mn2+-Doped Lead Halide Perovskite Nanocrystals with Dual-Color Emission Controlled by Halide Content. *J. Am. Chem. Soc.* **2016,** *138*, 14954-14961.

24. Liu, F.; Ding, C.; Zhang, Y. H.; Ripolles, T. S.; Kamisaka, T.; Toyoda, T.; Hayase, S.; Minemoto, T.; Yoshino, K.; Dai, S. Y.; Yanagida, M.; Noguchi, H.; Shen, Q., Colloidal Synthesis of Air-Stable Alloyed CsSn1-xPxI3 Perovskite Nanocrystals for Use in Solar Cells. *J. Am. Chem. Soc.* **2017,** *139*, 16708-16719.

25. Jellicoe, T. C.; Richter, J. M.; Glass, H. F. J.; Tabachnyk, M.; Brady, R.; Dutton, S. E.; Rao, A.; Friend, R. H.; Credgington, D.; Greenham, N. C.; Böhm, M. L., Synthesis and Optical Properties of Lead-Free Cesium Tin Halide Perovskite Nanocrystals. *J. Am. Chem. Soc.* **2016,** *138*, 2941-2944.

26. Dolzhnikov, D. S.; Wang, C.; Xu, Y.; Kanatzidis, M. G.; Weiss, E. A., Ligand-Free, Quantum-Confined Cs2SnI6 Perovskite Nanocrystals. *Chem. Mater.* **2017,** *29*, 7901-7907.

27. Udayabhaskararao, T.; Kazes, M.; Houben, L.; Lin, H.; Oron, D., Nucleation, Growth, and Structural Transformations of Perovskite Nanocrystals. *Chem. Mater.* **2017,** *29*, 1302-1308.

28. Liu, F.; Zhang, Y. H.; Ding, C.; Kobayashi, S.; Izuishi, T.; Nakazawa, N.; Toyoda, T.; Ohta, T.; Hayase, S.; Minemoto, T.; Yoshino, K.; Dai, S. Y.; Shen, Q., Highly Luminescent Phase-Stable CsPbI3 Perovskite Quantum Dots Achieving Near 100% Absolute Photoluminescence Quantum Yield. *ACS Nano* **2017,** *11*, 10373-10383.

29. Nedelcu, G.; Protesescu, L.; Yakunin, S.; Bodnarchuk, M. I.; Grotevent, M. J.; Kovalenko, M. V., Fast Anion-Exchange in Highly Luminescent Nanocrystals of Cesium Lead Halide Perovskites (CsPbX3, X = Cl, Br, I). *Nano Lett.* **2015,** *15*, 5635-5640.

30. Hazarika, A.; Zhao, Q.; Gaulding, E. A.; Christians, J. A.; Dou, B.; Marshall, A. R.; Moot, T.; Berry, J. J.; Johnson, J. C.; Luther, J. M., Perovskite Quantum Dot Photovoltaic Materials beyond the Reach of Thin Films: Full-Range Tuning of A-Site

Cation Composition. *ACS Nano* **2018,** *12*, 10327-10337.

31. Huang, H.; Chen, B. K.; Wang, Z. G.; Hung, T. F.; Susha, A. S.; Zhong, H. Z.; Rogach, A. L., Water Resistant CsPbX3 Nanocrystals Coated with Polyhedral Oligomeric Silsesquioxane and Their Use as Solid State Luminophores in All-Perovskite White Light-Emitting Devices. *Chem. Sci.* **2016,** *7*, 5699-5703.

32. Akkerman, Q. A.; D'Innocenzo, V.; Accornero, S.; Scarpellini, A.; Petrozza, A.; Prato, M.; Manna, L., Tuning the Optical Properties of Cesium Lead Halide Perovskite Nanocrystals by Anion Exchange Reactions. *J. Am. Chem. Soc.* **2015,** *137*, 10276-10281.

33. Li, Z.-J.; Hofman, E.; Davis, A. H.; Maye, M. M.; Zheng, W., General Strategy for the Growth of CsPbX3 (X = Cl, Br, I) Perovskite Nanosheets from the Assembly of Nanorods. *Chem. Mater.* **2018,** *30*, 3854-3860.

34. Lignos, I.; Stavrakis, S.; Nedelcu, G.; Protesescu, L.; Demello, A. J.; Kovalenko, M. V., Synthesis of Cesium Lead Halide Perovskite Nanocrystals in a Droplet-Based Microfluidic Platform: Fast Parametric Space Mapping. *Nano Lett.* **2016,** *16*, 1869-1877.

35. Liu, P.; Chen, W.; Wang, W.; Xu, B.; Wu, D.; Hao, J.; Cao, W.; Fang, F.; Li, Y.; Zeng, Y.; Pan, R.; Chen, S.; Cao, W.; Sun, X. W.; Wang, K., Halide-Rich Synthesized Cesium Lead Bromide Perovskite Nanocrystals for Light-Emitting Diodes with Improved Performance. *Chem. Mater.* **2017,** *29*, 5168-5173.

36. Imran, M.; Caligiuri, V.; Wang, M.; Goldoni, L.; Prato, M.; Krahne, R.; De Trizio, L.; Manna, L., Benzoyl Halides as Alternative Precursors for the Colloidal Synthesis of Lead-Based Halide Perovskite Nanocrystals. *J. Am. Chem. Soc.* **2018,** *140*, 2656-2664.

37. Woo, J. Y.; Kim, Y.; Bae, J.; Kim, T. G.; Kim, J. W.; Lee, D. C.; Jeong, S., Highly Stable Cesium Lead Halide Perovskite Nanocrystals through in Situ Lead Halide Inorganic Passivation. *Chem. Mater.* **2017,** *29*, 7088-7092.

38. Dong, Y.; Qiao, T.; Kim, D.; Parobek, D.; Rossi, D.; Son, D. H., Precise Control of Quantum Confinement in Cesium Lead Halide Perovskite Quantum Dots via Thermodynamic Equilibrium. *Nano Lett.* **2018,** *18*, 3716-3722.

39. Wharf, I.; Gramstad, T.; Makhija, R.; Onyszchuk, M., Synthesis and Vibrational Spectra of Some Lead (II) Halide Adducts with O-, S-, and N-Donor Atom Ligands. *Can. J. Chem.* **1976,** *54*, 3430-3438.

40. Lu, X. M.; Korgel, B. A.; Johnston, K. P., High Yield of Germanium Nanocrystals Synthesized from Germanium Diiodide in Solution. *Chem. Mater.* **2005,** *17*, 6479-6485.

41. Wheeler, L. M.; Sanehira, E. M.; Marshall, A. R.; Schulz, P.; Suri, M.; Anderson, N. C.; Christians, J. A.; Nordlund, D.; Sokaras, D.; Kroll, T.; Harvey, S. P.; Berry, J. J.; Lin, L. Y.; Luther, J. M., Targeted Ligand-Exchange Chemistry on Cesium Lead Halide Perovskite Quantum Dots for High-Efficiency Photovoltaics. *J. Am. Chem. Soc.* **2018,** *140*, 10504-10513.

42. De Roo, J.; Ibanez, M.; Geiregat, P.; Nedelcu, G.; Walravens, W.; Maes, J.; Martins, J. C.; Van Driessche, I.; Koyalenko, M. V.; Hens, Z., Highly Dynamic Ligand Binding and Light Absorption Coefficient of Cesium Lead Bromide Perovskite Nanocrystals. *ACS Nano* **2016,** *10*, 2071-2081.

43. Zhang, W.; Saliba, M.; Moore, D. T.; Pathak, S. K.; Horantner, M. T.; Stergiopoulos, T.; Stranks, S. D.; Eperon, G. E.; Alexander-Webber, J. A.; Abate, A.; Sadhanala, A.; Yao, S. H.; Chen, Y. L.; Friend, R. H.; Estroff, L. A.; Wiesner, U.; Snaith, H. J., Ultrasmooth Organic-Inorganic Perovskite Thin-Film Formation and Crystallization for Efficient Planar Heterojunction Solar Cells. *Nat. Commun.* **2015,** *6*, 6142.

44. De Wolf, S.; Holovsky, J.; Moon, S. J.; Loper, P.; Niesen, B.; Ledinsky, M.; Haug, F. J.; Yum, J. H.; Ballif, C., Organometallic Halide Perovskites: Sharp Optical Absorption Edge and Its Relation to Photovoltaic Performance. *J. Phys. Chem. Lett.* **2014,** *5*, 1035-1039.

45. Erslev, P. T.; Chen, H. Y.; Gao, J. B.; Beard, M. C.; Frank, A. J.; van de Lagemaat, J.; Johnson, J. C.; Luther, J. M., Sharp Exponential Band Tails in Highly Disordered Lead Sulfide Quantum Dot Arrays. *Phys. Rev. B* **2012,** *86*, 155313.

46. Liu, H. W.; Wu, Z. N.; Gao, H.; Shao, J. R.; Zou, H. Y.; Yao, D.; Liu, Y.; Zhang, H.; Yang, B., One-Step Preparation of Cesium Lead Halide CsPbX3 (X = CI, Br, and

I) Perovskite Nanocrystals by Microwave Irradiation. *ACS Appl. Mater. Inter.* **2017,** *9*, 42919-42927.

47. Klimov, V. I., Spectral and Dynamical Properties of Multiexcitons in Semiconductor Nanocrystals. *Annu. Rev. Phys. Chem.* **2007,** *58*, 635-673.

48. Robel, I.; Kuno, M.; Kamat, P. V., Size-Dependent Electron Injection from Excited CdSe Quantum Dots into TiO2 Nanoparticles. *J. Am. Chem. Soc.* **2007,** *129*, 4136-4137.

49. Liu, F.; Zhang, Y. H.; Ding, C.; Toyoda, T.; Ogomi, Y.; Ripolles, T. S.; Hayase, S.; Minemoto, T.; Yoshino, K.; Dai, S. Y.; Shen, Q., Ultrafast Electron Injection from Photoexcited Perovskite CsPbI3 QDs into TiO2 Nanoparticles with Injection Efficiency near 99%. *J. Phys. Chem. Lett.* **2018,** *9*, 294-297.

50. Makarov, N. S.; Guo, S.; Isaienko, O.; Liu, W.; Robel, I.; Klimov, V. I., Spectral and Dynamical Properties of Single Excitons, Biexcitons, and Trions in Cesium-Lead-Halide Perovskite Quantum Dots. *Nano Lett.* **2016,** *16*, 2349-2362.

51. Rainò, G.; Nedelcu, G.; Protesescu, L.; Bodnarchuk, M. I.; Kovalenko, M. V.; Mahrt, R. F.; Stöferle, T., Single Cesium Lead Halide Perovskite Nanocrystals at Low Temperature: Fast Single-Photon Emission, Reduced Blinking, and Exciton Fine Structure. *ACS Nano* **2016,** *10*, 2485-2490.

52. Park, Y.-S.; Guo, S.; Makarov, N. S.; Klimov, V. I., Room Temperature Single-Photon Emission from Individual Perovskite Quantum Dots. *ACS Nano* **2015,** *9*, 10386-10393.

53. Liu, Q.; Wang, Y.; Sui, N.; Wang, Y.; Chi, X.; Wang, Q.; Chen, Y.; Ji, W.; Zou, L.; Zhang, H., Exciton Relaxation Dynamics in Photo-Excited CsPbI3 Perovskite Nanocrystals. *Sci. Rep.* **2016,** *6*, 29442.

54. Sanehira, E. M.; Marshall, A. R.; Christians, J. A.; Harvey, S. P.; Ciesielski, P. N.; Wheeler, L. M.; Schulz, P.; Lin, L. Y.; Beard, M. C.; Luther, J. M., Enhanced Mobility CsPbI3 Quantum Dot Arrays for Record-Efficiency, High-Voltage Photovoltaic Cells. *Sci. Adv.* **2017,** *3*, eaao4204.

55. Franceschetti, A.; Zunger, A., Pseudopotential Calculations of Electron and Hole Addition Spectra of InAs, InP, and Si Quantum Dots. *Phys. Rev. B* **2000,** *62*,

2614-2623.

56. Leatherdale, C. A.; Bawendi, M. G., Observation of Solvatochromism in CdSe Colloidal Quantum Dots. *Phys. Rev. B* **2001,** *63*, 165315.

57. Liptay, W., Electrochromism and Solvatochromism. *Angew. Chem. Int. Ed.* **1969,** *8*, 177-188.

58. Liu, M. X.; Voznyy, O.; Sabatini, R.; de Arquer, F. P. G.; Munir, R.; Balawi, A. H.; Lan, X. Z.; Fan, F. J.; Walters, G.; Kirmani, A. R.; Hoogland, S.; Laquai, F.; Amassian, A.; Sargent, E. H., Hybrid Organic-Inorganic Inks Flatten the Energy Landscape in Colloidal Quantum Dot Solids. *Nat. Mater.* **2017,** *16*, 258-263.

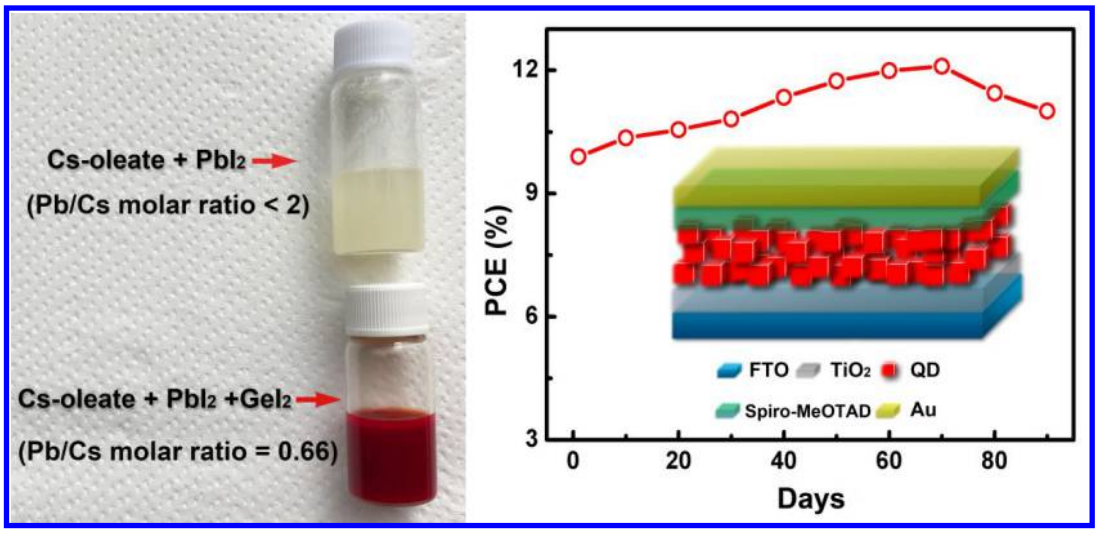

TOC